

**Assessing lower limb muscle parameters in
high-speed running on different surfaces using
inertial motion capture**

Gustav J. Chatterton

hst-22-idrtek-4-07



Aalborg Universitet
Kandidat i Idrætsteknologi
Kandidatspeciale 2022
Afleveringsdato: 01-06-2022



AALBORG UNIVERSITET
STUDENTERRAPPORT

Title: [Assessing lower limb muscle parameters in high-speed running on different surfaces using inertial motion capture]
Semester: [4th Semester]
Semester theme: [Masters]
Project period: [February - June]
ECTS: [30]
Supervisors: [Anderson de Souza Castelo Oliveira & Uwe G. Kersting]
Project group: [4-07]

Gustav Chatterton

[Gustav Johannes Chatterton]

Pages: [39]

Appendix: [4 pages]

ABSTRACT:

Studies investigating lower limb kinematics, kinetics and muscle parameters when performing high-speed running on natural grass, artificial grass and hard surfaces remain insufficient. Inertial motion capture and musculoskeletal modeling have proven a useful alternative to optical motion capture, for investigating muscle-tendon force, power, rate of length change and strain. Consequently, the aim of this study was to investigate the musculoskeletal differences for Biceps Femoris long head (BF_{lh}) and Semitendinosus (ST) when performing high-speed running on distinct/different surfaces. Twelve male/youth soccer players performed two 30-meter all out sprint tests on each surface, whilst obtaining kinematic recordings as input for the musculoskeletal modeling. The collected data was subject to a one-way repeated measures ANOVA which illustrated significant differences for BF_{lh} and ST power and rate of length change ($P < 0.05$). A post-hoc paired t-test exhibited significant differences in the following: ST power between natural grass and hard surfaces ($p < 0.001$); BF_{lh} rate of length change between natural grass and hard surfaces ($p = 0.023$) and ST rate of length change between natural grass and artificial grass ($p = 0.023$). No significant difference was found in force and strain. Running speed illustrated a significant difference when running on artificial grass compared to natural grass ($p = 0.02$). Running speed indicated to be the eminent variable differentiating when running on different surfaces. The higher running speed obtained on artificial grass is correlated with the differences in rate of length change and power.

Assessing lower limb muscle parameters in high-speed running on different surfaces using inertial motion capture

Gustav J. Chatterton^{1*}

¹Department of Health Science and Technology, Aalborg University, Fredrik Bajers vej 7 D2, 9000, Aalborg, Denmark

*Corresponding author. E-mail: Gchatt20@student.aau.dk

Abstract

Studies investigating lower limb kinematics, kinetics and muscle parameters when performing high-speed running on natural grass, artificial grass and hard surfaces remain insufficient. Inertial motion capture and musculoskeletal modeling have proven a useful alternative to optical motion capture, for investigating muscle-tendon force, power, rate of length change and strain. Consequently, the aim of this study was to investigate the musculoskeletal differences for Biceps Femoris long head (BF_{lh}) and Semitendinosus (ST) when performing high-speed running on distinct/different surfaces. Twelve male/youth soccer players performed two 30-meter all out sprint tests on each surface, whilst obtaining kinematic recordings as input for the musculoskeletal modeling. The collected data was subject to a one-way repeated measures ANOVA which illustrated significant differences for BF_{lh} and ST power and rate of length change ($P < 0.05$). A post-hoc paired t-test exhibited significant differences in the following: ST power between natural grass and hard surfaces ($p < 0.001$); BF_{lh} rate of length change between natural grass and hard surfaces ($p = 0.023$) and ST rate of length change between natural grass and artificial grass ($p = 0.023$). No significant difference was found in force and strain. Running speed illustrated a significant difference when running on artificial grass compared to natural grass ($p = 0.02$). Running speed indicated to be the eminent variable differentiating when running on different surfaces. The higher running speed obtained on artificial grass is correlated with the differences in rate of length change and power.

Keywords: Inertial motion capture, Inverse dynamics, Musculoskeletal modeling, Hamstring injuries, High-speed running.

1. Introduction:

Muscular injuries in highly intensive sports, such as soccer, are of increasing concern [1], [2]. Among these muscular injuries, lower limb injuries represent 92% of the total number of injuries, where 37% of these involve the hamstrings [1]. Magnetic resonance imaging performed after sustaining hamstring injuries illustrated that the majority are located to the Biceps Femoris long head (BFlh) [3]. Furthermore, by using musculoskeletal modeling and electromyography (EMG) in high-speed running, peak muscle-tendon force and strain was found for the BFlh and peak muscle-tendon rate of length change was discovered for Semitendinosus (ST) [4], [5]. The musculoskeletal differences between high-speed running on natural grass (NG), artificial grass (AG) and hard surfaces (HS), are to this day not well known, and further study regarding these differences are necessary for the advancement of hamstring injury research.

When investigating the effect of running on different surfaces, several parameters have been examined and show inconsistent results. Sassi et al., investigated the metabolic cost (i.e., $\text{J}\cdot\text{kg}^{-1}\cdot\text{m}^{-1}$) of running and found significant differences, meaning a higher physiological effort when running on NG and AG compared to HS [6]. Multiple studies have investigated the kinetic differences (i.e., ground reaction forces (GRF)), when running on distinct surfaces and with different shoes. The majority found no significant difference in GRF between the surfaces. Hence, the studies argue that lower extremity kinematic adaptations occur to obtain similar GRF's [7]–[9]. Sprint performance is related to surface traction, meaning that higher translational traction is beneficial for the acceleration phase. By utilizing the translational traction, the angle at which the resultant force is applied, is converted into a more horizontal force. Thereby, a higher traction allows the players to lean more forward into the movement and obtain higher horizontal accelerations [10], [11]. However, the injury risk related to translational surface traction show inconclusive results in the current literature but is affected by surface stiffness and vertical displacement related to the studs on the football boots [12]–[16].

Inertial motion capture (IMC) has proven to be a useful alternative to traditional optical motion capture (OMC) for in-field testing when measuring 3D segment kinematics [17], [18]. Recent studies have validated the use of IMC during high-speed running. By combining the IMC system with musculoskeletal modeling software, kinematics exhibited excellent correlations and varying relative root-mean-square errors (knee: $\rho=0.98$, $r\text{RMSE}=21.0\%$, hip: $\rho=0.95$, $r\text{RMSE}=18.5\%$, ankle: $\rho=0.93$, $r\text{RMSE}=46.6\%$). Furthermore, GRF predictions illustrated varying results (anteroposterior: $\rho=0.77$,

rRMSE=33.4%, mediolateral: $\rho=0.04$, rRMSE=69.1%, vertical: $\rho=0.78$, rRMSE=25.7%). Combined, IMC was proposed as a useful alternative to OMC and force plates for the lower limb estimations [19]. Furthermore, IMC together with musculoskeletal modeling facilitates the estimation of joint reaction forces and muscle parameters [20]. This includes estimations of parameters that are not measurable without invasive methods, such as muscle-tendon force, muscle power and muscle-tendon strain.

The mentioned estimations have, through animal studies, been proven to be an important parameter related to the damage of the strained muscle during eccentric contractions [5], [21]. Thereby, IMC combined with musculoskeletal modeling allows the acquisition of in-field kinematics, kinetic and muscle parameters of soccer players in their natural environment during high-speed running, substantially increasing the ecological validity of the research outcomes.

Therefore, the aim of the study was to investigate if hamstring muscle parameters (i.e., muscle-tendon force, power, rate of length change and strain) diverge, when performing high-speed running on NG, AG, and HS. Hence, it was hypothesized that high-speed running on NG with football boots would induce higher peak muscle-tendon force, power, muscle-tendon rate of length change and strain compared to high-speed running on AG with football boots and on HS with running shoes. Furthermore, it was hypothesized that high-speed running on AG with football boots would produce higher peak values than high-speed running on HS with running shoes. Additionally, it was hypothesized that BFlh would exhibit higher peak muscle force, power and strain compared to ST. However, ST would produce higher peak muscle-tendon rate of length change than BFlh.

2. Methods

2.1 Participants:

Twelve male youth soccer players with no history of hamstring injuries the previous 6 months and no present musculoskeletal or neuromuscular disorder were recruited for the study (age: 18.2 years \pm 1.15, height: 1.80 m \pm 0.07, weight: 64.4 Kg \pm 9.4, body mass index (BMI): 21.2 \pm 1.91). All participants were physically active, played in the top Danish U19 or second U19 league and performed three to five training sessions per week. The experimental data were recorded at FC Midtjylland's training facilities in Ikast, Denmark. The tests were performed in accordance with the ethical guidelines of the ethical committee of Region North Jutland, Denmark. Preliminary to the tests, subjects were informed of the protocol and provided full written consent.

2.2 Experimental protocol

In a single session, participants performed 30-meter sprints on NG, AG, and HS. The subjects used football boots when running on NG and AG and running shoes on HS. The artificial grass type was the Saltex Drop MTRX 40 with Bionic Fiber (Unisport Scandinavia ApS, Silkeborg, Denmark). The subjects were equipped with an IMC system, followed by a short warm-up protocol conducted by the physical trainer of the team. Subsequently, in a randomized order, subjects performed two maximal sprints on the 30-meter track on NG, AG, and HS, while full-body kinematics using the IMC-system were acquired. Between trials, one minute of rest was held per active second, to minimize the impact of fatigue. Two trials on each surface were recorded. A trial was accepted when two successive strides of the dominant leg were recorded within the 30-meter track. Trials with visually poor IMC recordings were excluded and a new trial was acquired.

2.3 Instrumentation:

The IMC system used to capture full-body kinematics was the Xsens MVN Link (Xsens Technologies BV, Enschede, The Netherlands) and its software (Xsens MVN Studio version 4.2.4, Xsens Technologies BV, Enschede, The Netherlands), which sampled data at 240 Hz. Seventeen IMUs were located at the head, sternum, pelvis, upper legs, lower legs, feet, shoulders, upper arms, forearms, and hands (Figure 1). The IMUs were placed in a full-body suit, enabling fixation to the specific placement, and thereby minimizing the movement of the IMU relative to its original position. Running speed was obtained with Brower Timing Gates TCi System (Brower Timing Systems LLC, Draper, UT, USA).

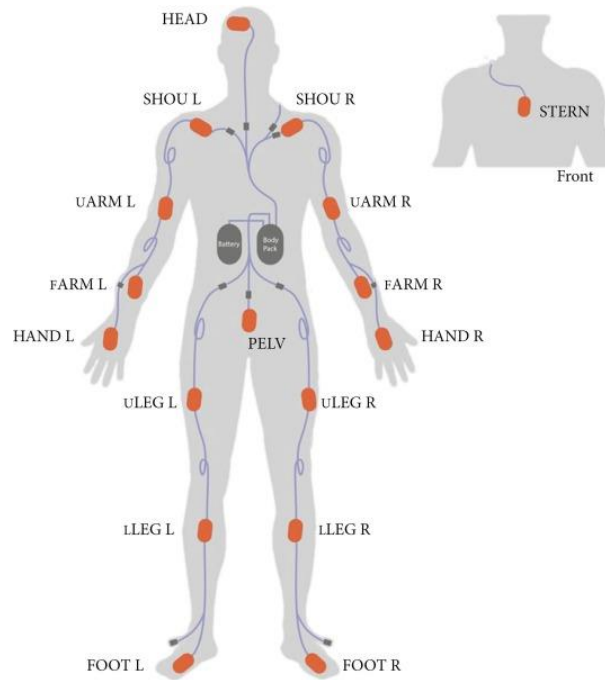


Fig.1. The placement of the 17 IMUs defining the specific segments of the Xsens MVN model [22].

2. 4 Musculoskeletal model

A musculoskeletal model was constructed in a musculoskeletal modeling software (AnyBody Modeling System v. 7.3, AnyBody Technology A/S, Aalborg, Denmark) and based on the AnyMocap framework. The BVH_Xsens template was extracted from the AnyBody Model Repository v. 2.3. The provided model was based on different studies defining geometry and parameter settings for the different segments of the body. The shoulder and upper limb models were provided by Veeger et al. and Van der Helm et al.[23], [24], the lumbar spine model was based on de Zee et al. [25], Hansen et al.[26], and Han et al.[27], and finally, the lower extremity model was based on Carbone et al. [28]. Thereby, the model encased 44 degrees-of-freedom (DOF) containing 2 x 3 DOF at the ankles, 2 x 1 at the knees, 2 x 3 at the hip, 6 DOF at the pelvis, 3 DOF between thorax and pelvis, 2 x 2 at the elbows, 2 x 3 at the glenohumeral, 2 x 3 at the sternoclavicular, 2 x 2 DOF at the wrists and 1 DOF at the neck.

2.5 IMC model scaling

Prior to testing, the participants were instructed to perform the final calibration of the IMC system. This consisted of standing in a neutral position (N-pose), followed by a short walk, and returning to the N-pose. When the calibration was accepted a short walk was performed for final synchronization.

Before the first 30-meter sprint on each surface, a standing reference trial with a N-pose was conducted, to identify the original segment lengths. The kinematic data recorded by the IMC system, provided the definition of 23 body segments as described by Karatsidis et al. [17]. The body dimensions used as input for the musculoskeletal models, were obtained following the IMC system guidelines.

To enable scaling of these segments, a stick figure was generated in Xsens MVN studio. Subsequently, a bvh-file containing both the kinematic data and the stick figure were imported to the musculoskeletal modeling software. By using AnyBody's BVH_Xsens model as a template, virtual markers were introduced to the stick figures according to the joint-to-joint distances, thereby enabling the scaling of the BVH Xsens model segment dimensions. However, the pelvis, foot, and trunk segments from the stick figure, could not be directly scaled. Thereby, additional markers based on the least-squares minimization method were introduced, enabling a scaling of the final model. The mass of each segment was determined linearly by the total body mass of the subject, using Winter's segment to mass ratio equations [29].

To enable GRF prediction, the musculoskeletal model was adjusted by the method introduced by Skals et al.[30]. Hereby, 25 dynamic contact nodes were attached under each foot, each consisting of five uniaxial force actuators. To establish activation of the contact nodes, when the foot was near the ground, a height and velocity threshold was set to 0.04 m and 2.00 m/s, respectively. The nodes generated a positive vertical force perpendicular to the ground and static friction forces in the anteroposterior and mediolateral direction. Running on different surfaces with specific shoe wear, generates distinct friction coefficients. Shorten & Himmelsbach evaluated different shoe wear on four distinct surfaces and illustrated friction coefficient of 0.5 for HS, 0.95 for NG and 1.3 for AG, which was implemented the current study [11].

2.6 Muscle recruitment:

To estimate joint reaction force, joint moments and muscle forces, a muscle recruitment problem must be solved. Hence, the following polynomial optimization problem is defined;

$$G(f^M) = \sum_{i=1}^{n^{(M)}} \left(\frac{f_i^{(M)}}{N_i} \right)^2$$

$$Cf = d$$

$$0 \leq f_i^{(M)} \leq N_i, i = 1 \dots, n^{(M)}$$

To obtain numerical stability a second-order quadratic minimization function, G , was formulated. The function is defined by $f_i^{(M)}$ which is the i 'th muscle force, N_i indicates the strength of the i 'th muscle and $n^{(M)}$ expresses the number of muscles. The function is constrained by dynamic equilibrium equations and $f^{(M)}$ which contain non-negativity conditions, establishing that muscles only can pull and not push. Additionally, the muscle force $f_i^{(M)}$ is constricted to remain below its strength N_i . Furthermore, a coefficient matrix, C , embraces the dynamic equilibrium and the vector f expresses all unknown joint reaction- and muscle forces. To obtain equilibrium, d contain all external loads and internal forces [17], [30], [31]. The strength of the muscles used to drive the model, were based on previous studies describing the different segments. If the strength were held stationary the maximal muscle forces were considered constant for the different muscle lengths and contraction velocities [23]–[25]. The muscle strength was then adjusted using a scaling factor based on Body-Mass-Index as described by Frankenfield et al. [32].

2.7 Data analysis

Following the implementation of the BVH-file incorporating the kinematic data and the stick figure to the AnyBody software, the inertial marker trajectories were low-pass filtered (2nd order, 15 Hz Butterworth). Subsequently, the following muscle parameters for ST and BFlh were derived: muscle-tendon force output (F_{out}), muscle-tendon power (P_{mt}), length of the muscle-tendon unit (L_{mt}) and muscle-tendon unit rate of length change (L_{mtDot}). F_{out} was expressed in the optimization function(s) and is a product of all internal and external forces. P_{mt} is defined as the product of F_{out} and L_{mtDot} . L_{mtDot} is expressed as the first derivative of L_{mt} with respect to time [5]. Furthermore, L_{mt} was computed as percent strain by utilizing the standing reference trial. All muscle parameters were extracted for two full gait cycles for the dominant leg (i.e., foot strike to foot strike), in the 30 m sprint without participants alternating their running style. For further analysis all parameters were imported to a customized script in Spyder v.5 scientific Python development environment. Five of the participants were left leg dominant, meaning an adjustment of the force direction of the GRF prediction. For an appropriate comparison between surfaces, subjects and trials, several normalization steps were introduced. Firstly, the time axis for the muscle parameters were set to 100 % of the gait cycle. Secondly, F_{out} and P_{mt} were normalized to body weight (BW) and Watt/Kg (W/Kg). For further statistical analysis, the data from each participant were computed as subject specific means of all trials on each specific surface. For visual representation of all muscle parameters Seaborn line plots with mean and standard deviation were constructed. For statistical comparisons between the

three surfaces, one-dimensional statistical parametric mapping (SPM) was established for all muscle parameters (i.e., Fout, Pmt, LmtDot and strain). By conducting a one-way ANOVA with repeated measures, SPM allows the comparison by calculating traditional F statistics (i.e., SPM {F}) in a continuous time series [33]. If a significant difference was found between the three conditions, a post-hoc paired t-test was conducted, for pairwise comparison. The effect of the surface on running speed was accessed through a paired t-test. The significance level was set at $p < 0.05$ for all statistical tests.

Peak values for each muscle parameter were computed as subject specific means across the three surfaces and between the two hamstring muscles. For comparison, SNS violin plots were constructed, which allows the same statistical measures as regular boxplots (i.e., interquartile range and adjacent values), but simultaneously incorporates the data distribution by density plots [34].

3. Results

3.1 Results

Twenty-four trials on each surface were recorded, meaning a total 72 trials of which six were excluded due to adverse weather conditions. Two full gait cycles were extracted for each participant on every surface. Thereby, 132 gait cycles were incorporated in the results.

3.2 Running speed

The average running speed on the three surfaces was: $6.69 \text{ m/s} \pm 0.32$ on NG, $6.75 \text{ m/s} \pm 0.31$ on HS and $6.89 \text{ m/s} \pm 0.28$ on AG (Figure 2). A significant difference was found between NG and AG ($P = 0.02$). No significant differences were found between the other conditions ($P > 0.05$).

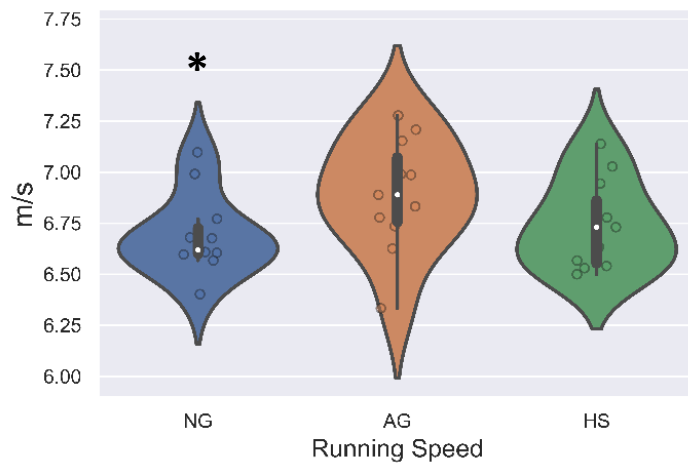


Fig. 2 Violin plots illustrating median, interquartile range, adjacent values and data distribution for peak running speed (m/s) for all three surfaces; Natural grass (NG), Artificial grass (AG) and Hard surface (HS). * Denotes significant difference in relation to AG ($P = 0.02$).

3.3 Muscle force (Fout)

The one-way ANOVA with repeated measures illustrated no significant differences between the three surfaces for the BF1h (Figures 3A and 3B) and ST (Figures 3C and 3D) muscle Fout ($p > 0.05$). Fout exhibited higher peak values and variance at the terminal swing phase for both BF1h and ST.

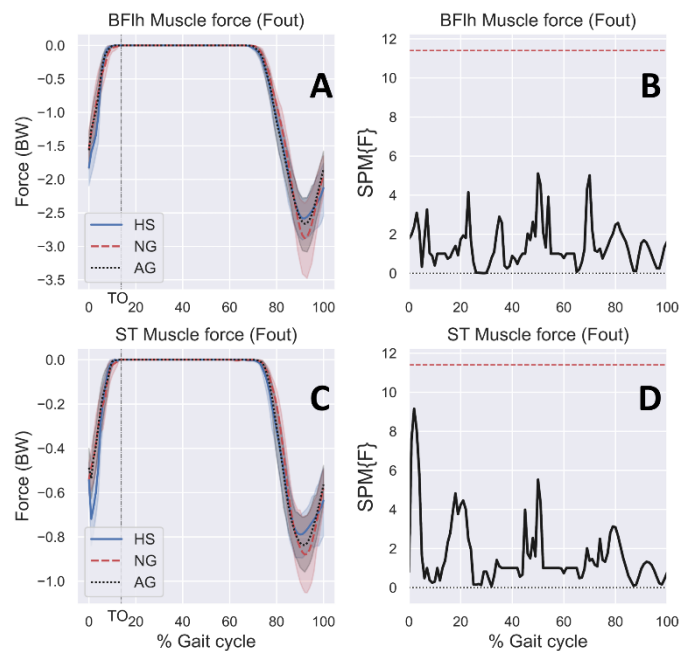


Fig. 3 Mean, SD and SPM from BF1h and ST muscle force (Fout). The vertical axis for the mean (SD) plots are normalized to force (BW) and the horizontal axis is normalized to 100 % gait cycle. TO indicates the toe-offset in the gait cycle.

3.4 Muscle power (Pmt)

A significant difference was found for the BFlh Pmt (Figure 4A and 4B) from 0 to 3% of the gait cycle ($p < 0.001$) and for the ST Pmt (Figures 4C and 4D) from 0 to 4% ($p < 0.001$). The post-hoc paired t-test showed significant difference in ST Pmt between NG and HS ($p < 0.001$). However, no significant difference was found for the BFlh Pmt in the post-hoc analysis.

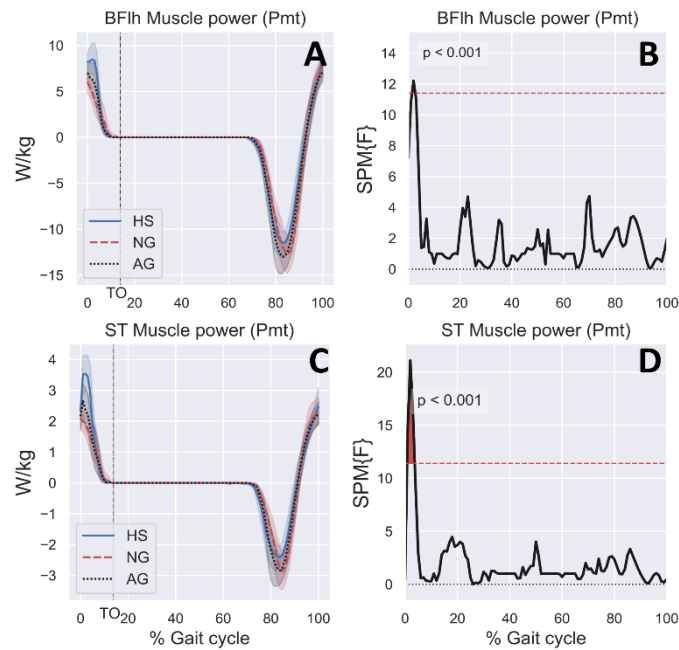


Fig. 4 Mean, SD, and SPM from BFlh and ST muscle power (Pmt). The vertical axis for the mean (SD) plots are normalized to power (W/kg) and the horizontal axis is normalized to 100 % gait cycle.

3.5 Muscle-tendon rate of length change (LmtDot)

Significant differences were exhibited for the BFlh LmtDot (Figures 5A and 5B) from 3 to 10% ($p = 0.016$) and for the ST LmtDot (Figure 5C and 5D) from 4 to 11% and 20 to 25% ($p = 0.016$ and $p = 0.015$). The post-hoc paired t-test showed significant difference between NG and HS at BFlh LmtDot ($p = 0.023$) and for ST LmtDot between NG and AG ($p = 0.023$).

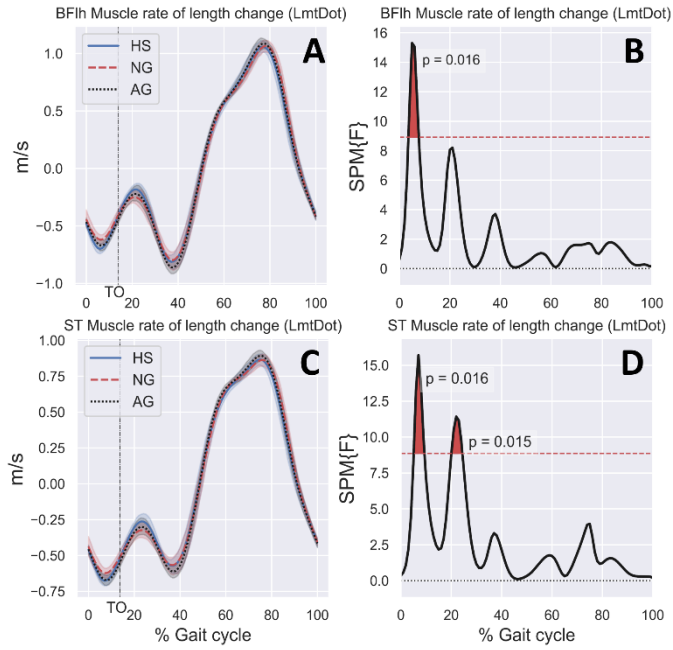


Fig. 5 Mean, SD, and SPM from BFlh and ST muscle-tendon rate of length change. The vertical axis for the mean (SD) plots are normalized to m/s and the horizontal axis is normalized to 100% gait cycle.

3.6 Muscle strain

The ANOVA test showed no significant differences across the whole gait cycle for both the BFlh and ST muscle strain (Figures 6A, 6B, 6C and 6D).

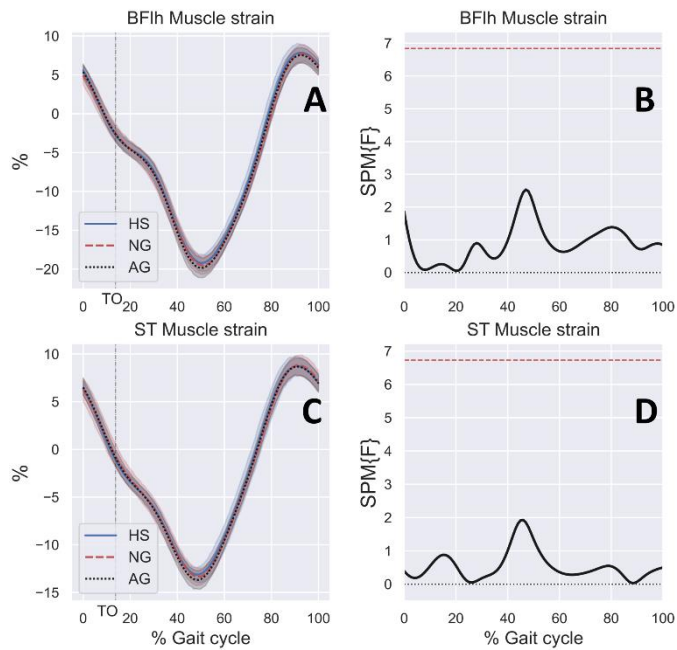


Fig. 6 Mean, SD, and SPM from BF_{lh} and ST muscle strain. The vertical axis for the mean (SD) plots are normalized to percent (%) and the horizontal axis is normalized to 100 % gait cycle.

3.7 Peak values

A paired t-test illustrated a significant difference between the peak values from all muscle parameters when comparing BF_{lh} with ST ($P < 0.05$). When evaluating the effect of the surfaces, Fout (Fig 7A and 7B) showed no considerable difference in interquartile range. However, NG illustrated a higher tendency to produce outliers for both BF_{lh} and ST. Pmt (Figures 7C and 7D), LmtDot (Figures 7E and 7F) and strain (Figures 7G and 7H) all exhibited similar interquartile ranges, adjacent values, and data distribution across all surfaces for both BF_{lh} and ST.

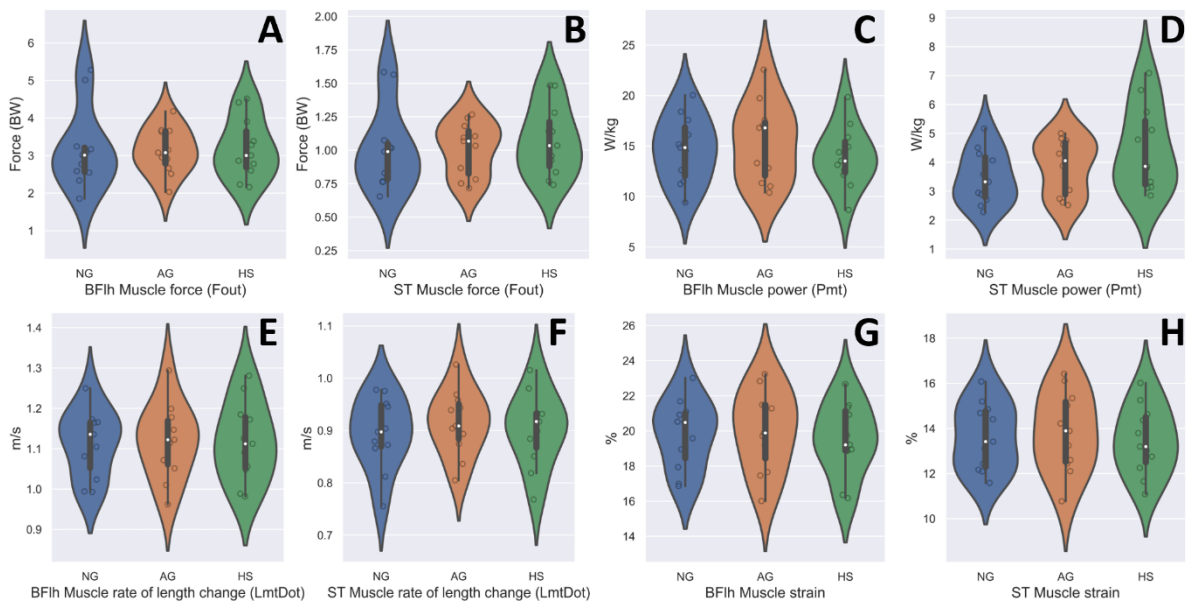


Fig 7. Violin plots illustrating median, interquartile range, adjacent values, and data distribution for the BF_{lh} and ST, across all surfaces; NG (blue), AG (orange) and HS (green).

4. Discussion

The objective of the current study was to examine if BFlh and ST muscle parameters (i.e., Fout, Pmt, LmtDot and strain) for soccer players differentiated when performing high-speed running on NG, AG, and HS. The eminent findings were significant differences for ST Pmt ($p < 0.001$), along with a significant difference for both BFlh and ST LmtDot between the surfaces ($p = 0.023$). Additionally, when comparing all muscle parameters on each surface BFlh exhibited significant higher peak values opposed to ST ($P < 0.05$). Furthermore, running speed on NG was significantly slower when compared with AG ($P = 0.02$). Thereby, the results illustrate that running on different surfaces induces different running speeds, which further produces an effect on the muscle parameters.

The differences found in LmtDot for both ST and BFlh are found in the stance phase, where a higher LmtDot on average is found on HS compared to NG for BFlh and on AG compared to NG for ST. The differences found in the post-hoc analysis in Pmt for ST and in the one-way ANOVA for BFlh, when performing high-speed running on different surfaces, are related to the results of LmtDot. Pmt is the product of Fout and LmtDot and even though no difference was found in Fout, the difference in LmtDot influences Pmt. Thereby, it could be argued that when running on different surfaces with distinct properties (i.e., stiffness) a kinematic adaptation takes place, which results in modified knee- and hip angle or angular velocity. This corresponds to the previous studies which found no significant difference in GRF and argued that kinematic adaptation took place during the gait cycle [7]–[9].

The higher Pmt found on HS compared to NG for ST, was exhibited in the stance phase. These effects are contradictory to prior studies investigating the difference in running on distinct surfaces. Sassi et al. illustrated a higher metabolic cost of running, when running on NG compared to AG and HS. Hence, it was argued that a higher metabolic cost of running was related to a combination of the surface shock absorption and the footwear [6]. The effects in the study by Sassi et al., were however found under controlled running speeds. Subsequently, the effect of different running speeds on both LmtDot and Pmt was excluded. In the present study participants were instructed to perform a maximal effort sprint on each surface, which thereby would allow the possibility to obtain higher velocities on one surface compared to others. NG (6.69 m/s) was significantly slower compared to AG (6.89 m/s) and moderately slower compared to HS (6.75 m/s). A higher running speed is linked to a higher angular velocity, meaning the possibility of a higher LmtDot. Since Pmt is dependent on LmtDot, it is arguable that a higher velocity during the stance phase would result in a higher Pmt. Furthermore, running speed is associated with a higher metabolic cost, indicating that obtaining higher velocities also is an important factor when evaluating both the metabolic cost and Pmt [35].

The higher running speed on AG compared to NG and HS relates to altered surface traction. The friction coefficient set on AG (1.3) compared to HS (0.5) and NG (0.95) is higher. A higher translational traction allows the possibility to lower the angle at which the resultant force is applied to the ground. Thereby, the higher translational traction on AG allows the participants to accelerate faster without losing traction compared to the other surfaces [10], [11].

Furthermore, if a lower angle between the body and surfaces is obtained, it would result in a kinematic adaptation for the knee and hip. A larger hip flexion and a larger knee extension would result in a higher strain of the muscles [36]. However, this study did not find any significant differences for strain in the terminal swing phase, indicating that additional variables are needed to fully interpret the results. Force is the result of mass multiplied by acceleration, indicating that the acceleration of the shank and the velocity of the knee extension in the terminal swing phase, would be of great interest when investigating the kinematic adaptations [4].

Increased running speed has been associated with higher risks of hamstring injuries, due to an increased amount of negative work performed in the muscle in the terminal swing phase [4]. However, in the current study NG displayed the slowest running speeds of all three surfaces. By visual inspection (Figures 3A and 3C), Fout displayed more outliers for both ST and BFlh in the terminal swing phase when running on NG compared to AG and HS. This thereby indicates that high-speed running on NG is associated with higher Fout values in the terminal swing phase and would again indicate that kinematic adaptations take place.

The higher peak muscle-tendon Fout, Pmt and strain for BFlh compared to ST are in correspondence with the results of Schache et al. [5]. However, the higher LmtDot found for BFlh contradicts the findings of Schache et al. These contradictory results can be explained by numerous explanations, such as study population, surface- and footwear type etc. One argument would be the accuracy and reliability of IMC systems and musculoskeletal modeling. Multiple studies have investigated and validated the IMC system combined with musculoskeletal modeling in different movements [17]–[20]. However, investigating muscle parameters in high-speed running, presents a greater challenge for data acquisitions when compared to other movement types. Hence, further studies investigating the accuracy of IMC combined with musculoskeletal modeling in soccer environments are needed.

The present study was subject to several limitations that could have affected the results and investigation. First, the friction coefficients used for the musculoskeletal modeling were estimates obtained by visually inspecting a graph in the study by Shorten & Himmelsbach [11]. It would have

been ideal to use specific values of friction for each combination of surface and shoe. However, acquiring a friction coefficient between NG, AG and HS and different shoes, is troublesome due to inconsistencies in both turf and shoe surface. Second, the surface stiffness was not incorporated in the musculoskeletal modeling. By incorporating the stiffness of the surfaces, it could have led to different results in the stance phase. However, the majority of studies investigating GRFs, do not find any impact of the surface stiffness [7]–[9]. Third, the participants wore different football boots and running shoes. Hence, different shoe/surface interactions would take place between the participants, meaning that distinct frictions and stiffnesses have affected the results [12]. Finally, by using IMC and musculoskeletal modeling to investigate muscle parameters, only indirect measurements are obtained. Thereby, a direct measurement of the muscle activity performed by EMG would have enhanced the validity of the study.

Future research should investigate the effect that friction and surface stiffness would have on the muscle parameters. An implementation of surface stiffness in the musculoskeletal modeling would require both coding in AnyBody and examining the stiffness properties of each surface used in the study. Additionally, to enhance the accuracy of the musculoskeletal modeling, future work should consider using OMC and if possible, force plates to obtain kinematic and kinetic measurements. Last, the results of the musculoskeletal modeling could be confirmed by incorporating the direct measurement of muscle activity with EMG.

5. Conclusion

This study showed that when performing high-speed running on three different surfaces, modifications in muscle-tendon power (Pmt), muscle-tendon rate of length change (LmtDot) and running speed occur. The significant difference in LmtDot exhibited in the stance phase is related to an increased running speed on surfaces with both higher traction and stiffness, which further affects the Pmt. No significant effects were found for muscle-tendon force (Fout) and muscle-tendon strain for both Biceps Femoris long head (BF_{lh}) and Semitendinosus (ST). Additionally, significant differences for all muscle parameters were exhibited when comparing BF_{lh} with ST.

Hence, it can be concluded when running on artificial grass (AG) and hard surface (HS) compared to natural grass (NG), a higher velocity in the stance phase is associated with a higher LmtDot and Pmt.

References

- [1] J. Ekstrand, M. Häggglund, and M. Waldén, “Epidemiology of Muscle Injuries in Professional Football (Soccer),” *Am. J. Sports Med.*, vol. 39, no. 6, pp. 1226–1232, Jun. 2011, doi: 10.1177/0363546510395879.
- [2] J. Ekstrand, M. Waldén, and M. Häggglund, “Hamstring injuries have increased by 4% annually in men’s professional football, since 2001: a 13-year longitudinal analysis of the UEFA Elite Club injury study,” *Br. J. Sports Med.*, vol. 50, no. 12, pp. 731–737, Jun. 2016, doi: 10.1136/bjsports-2015-095359.
- [3] C. M. Askling, M. Tengvar, T. Saartok, and A. Thorstensson, “Acute First-Time Hamstring Strains during Slow-Speed Stretching: Clinical, Magnetic Resonance Imaging, and Recovery Characteristics,” *Am. J. Sports Med.*, vol. 35, no. 10, pp. 1716–1724, Oct. 2007, doi: 10.1177/0363546507303563.
- [4] E. S. Chumanov, B. C. Heiderscheit, and D. G. Thelen, “Hamstring Musculotendon Dynamics during Stance and Swing Phases of High-Speed Running,” *Med. Sci. Sports Exerc.*, vol. 43, no. 3, pp. 525–532, Mar. 2011, doi: 10.1249/MSS.0b013e3181f23fe8.
- [5] A. G. Schache, T. W. Dorn, P. D. Blanch, N. A. T. Brown, and M. G. Pandy, “Mechanics of the Human Hamstring Muscles during Sprinting,” *Med. Sci. Sports Exerc.*, vol. 44, no. 4, pp. 647–658, Apr. 2012, doi: 10.1249/MSS.0b013e318236a3d2.
- [6] A. Sassi, A. Stefanescu, P. Menaspa’, A. Bosio, M. Riggio, and E. Rampinini, “The Cost of Running on Natural Grass and Artificial Turf Surfaces,” *J. Strength Cond. Res.*, vol. 25, no. 3, pp. 606–611, Mar. 2011, doi: 10.1519/JSC.0b013e3181c7baf9.
- [7] S. J. Dixon, A. C. Collop, and M. E. Batt, “Surface effects on ground reaction forces and lower extremity kinematics in running:,” *Med. Sci. Sports Exerc.*, vol. 32, no. 11, pp. 1919–1926, Nov. 2000, doi: 10.1097/00005768-200011000-00016.
- [8] E. C. Hardin, A. J. Van Den Bogert, and J. Hamill, “Kinematic Adaptations during Running: Effects of Footwear, Surface, and Duration:,” *Med. Sci. Sports Exerc.*, pp. 838–844, May 2004, doi: 10.1249/01.MSS.0000126605.65966.40.
- [9] N. A. A. A. Yamin, M. A. Amran, K. S. Basaruddin, A. F. Salleh, and W. M. R. Rusli, “Ground reaction force response during running on different surface hardness,” *ARPN J. Eng. Appl. Sci.*, vol. 2017, 2017.
- [10] G. Luo and D. Stefanyshyn, “Identification of critical traction values for maximum athletic performance,” *Footwear Sci.*, vol. 3, no. 3, pp. 127–138, Sep. 2011, doi: 10.1080/19424280.2011.639807.
- [11] M. R. Shorten and J. A. Himmelsbach, “Shorten, M.R., Hudson, B., & Himmelsbach, J.A. (2002). SHOE-SURFACE TRACTION OF CONVENTIONAL AND IN-FILLED SYNTHETIC TURF FOOTBALL SURFACES,” 2002.
- [12] J. D. Clarke and M. J. Carré, “Improving the performance of soccer boots on artificial and natural soccer surfaces,” *Procedia Eng.*, vol. 2, no. 2, pp. 2775–2781, Jun. 2010, doi: 10.1016/j.proeng.2010.04.065.
- [13] J. L. Dragoo and H. J. Braun, “The Effect of Playing Surface on Injury Rate: A Review of the Current Literature,” *Sports Med.*, vol. 40, no. 11, pp. 981–990, Nov. 2010, doi: 10.2165/11535910-000000000-00000.
- [14] J. Wannop, “Footwear traction and lower extremity non-contact injury,” 2012, doi: 10.11575/PRISM/26204.
- [15] J. W. Wannop, G. Luo, and D. J. Stefanyshyn, “Footwear traction at different areas on artificial and natural grass fields,” *Sports Eng.*, vol. 15, no. 2, pp. 111–116, Jun. 2012, doi: 10.1007/s12283-012-0091-x.

- [16] E. M. Zanetti, C. Bignardi, G. Franceschini, and A. L. Audenino, "Amateur football pitches: Mechanical properties of the natural ground and of different artificial turf infills and their biomechanical implications," *J. Sports Sci.*, vol. 31, no. 7, pp. 767–778, Apr. 2013, doi: 10.1080/02640414.2012.750005.
- [17] A. Karatsidis, G. Bellusci, H. Schepers, M. de Zee, M. Andersen, and P. Veltink, "Estimation of Ground Reaction Forces and Moments During Gait Using Only Inertial Motion Capture," *Sensors*, vol. 17, no. 12, p. 75, Dec. 2016, doi: 10.3390/s17010075.
- [18] J.-T. Zhang, A. C. Novak, B. Brouwer, and Q. Li, "Concurrent validation of Xsens MVN measurement of lower limb joint angular kinematics," *Physiol. Meas.*, vol. 34, no. 8, pp. N63–N69, Aug. 2013, doi: 10.1088/0967-3334/34/8/N63.
- [19] G. J. Chatterton, J. B. Hansen, N. H. Kristiansen, N. P. Kunwald, U. G. Kersting, and A. S. Oliveira, "ASSESSING KINEMATICS AND KINETICS OF HIGH-SPEED RUNNING USING INERTIAL MOTION CAPTURE: A PRELIMINARY ANALYSIS," *ISBS Proceedings Archive*, vol. 2022, Appendix A.
- [20] F. G. Larsen, F. P. Svenningsen, M. S. Andersen, M. de Zee, and S. Skals, "Estimation of Spinal Loading During Manual Materials Handling Using Inertial Motion Capture," *Ann. Biomed. Eng.*, vol. 48, no. 2, pp. 805–821, Feb. 2020, doi: 10.1007/s10439-019-02409-8.
- [21] R. L. Lieber and J. Friden, "Muscle damage is not a function of muscle force but active muscle strain," *J. Appl. Physiol.*, vol. 74, no. 2, pp. 520–526, Feb. 1993, doi: 10.1152/jappl.1993.74.2.520.
- [22] F. P. Svenningsen, M. de Zee, and A. S. Oliveira, "The effect of shoe and floor characteristics on walking kinematics," *Hum. Mov. Sci.*, vol. 66, pp. 63–72, Aug. 2019, doi: 10.1016/j.humov.2019.03.014.
- [23] F. C. T. Van der Helm, H. E. J. Veeger, G. M. Pronk, L. H. V. Van der Woude, and R. H. Rozendal, "Geometry parameters for musculoskeletal modelling of the shoulder system," *J. Biomech.*, vol. 25, no. 2, pp. 129–144, Feb. 1992, doi: 10.1016/0021-9290(92)90270-B.
- [24] H. E. Veeger, B. Yu, K. N. An, and R. H. Rozendal, "Parameters for modeling the upper extremity," *J. Biomech.*, vol. 30, no. 6, pp. 647–652, Jun. 1997, doi: 10.1016/s0021-9290(97)00011-0.
- [25] M. de Zee, L. Hansen, C. Wong, J. Rasmussen, and E. B. Simonsen, "A generic detailed rigid-body lumbar spine model," *J. Biomech.*, vol. 40, no. 6, pp. 1219–1227, 2007, doi: 10.1016/j.jbiomech.2006.05.030.
- [26] L. Hansen, M. de Zee, J. Rasmussen, T. B. Andersen, C. Wong, and E. B. Simonsen, "Anatomy and biomechanics of the back muscles in the lumbar spine with reference to biomechanical modeling," *Spine*, vol. 31, no. 17, pp. 1888–1899, Aug. 2006, doi: 10.1097/01.brs.0000229232.66090.58.
- [27] K.-S. Han, T. Zander, W. R. Taylor, and A. Rohlmann, "An enhanced and validated generic thoraco-lumbar spine model for prediction of muscle forces," *Med. Eng. Phys.*, vol. 34, no. 6, pp. 709–716, Jul. 2012, doi: 10.1016/j.medengphy.2011.09.014.
- [28] V. Carbone *et al.*, "TLEM 2.0 - a comprehensive musculoskeletal geometry dataset for subject-specific modeling of lower extremity," *J. Biomech.*, vol. 48, no. 5, pp. 734–741, Mar. 2015, doi: 10.1016/j.jbiomech.2014.12.034.
- [29] D. A. Winter, *Biomechanics and motor control of human movement*, 4th ed. Hoboken, N.J: Wiley, 2009.
- [30] S. Skals, M. K. Jung, M. Damsgaard, and M. S. Andersen, "Prediction of ground reaction forces and moments during sports-related movements," *Multibody Syst. Dyn.*, vol. 39, no. 3, pp. 175–195, Mar. 2017, doi: 10.1007/s11044-016-9537-4.

- [31] M. Damsgaard, J. Rasmussen, S. T. Christensen, E. Surma, and M. de Zee, “Analysis of musculoskeletal systems in the AnyBody Modeling System,” *Simul. Model. Pract. Theory*, vol. 14, no. 8, pp. 1100–1111, Nov. 2006, doi: 10.1016/j.simpat.2006.09.001.
- [32] D. C. Frankenfield, W. A. Rowe, R. N. Cooney, J. S. Smith, and D. Becker, “Limits of body mass index to detect obesity and predict body composition,” *Nutr. Burbank Los Angel. Cty. Calif*, vol. 17, no. 1, pp. 26–30, Jan. 2001, doi: 10.1016/s0899-9007(00)00471-8.
- [33] T. C. Pataky, “Generalized n-dimensional biomechanical field analysis using statistical parametric mapping,” *J. Biomech.*, vol. 43, no. 10, pp. 1976–1982, Jul. 2010, doi: 10.1016/j.jbiomech.2010.03.008.
- [34] J. L. Hintze and R. D. Nelson, “Violin Plots: A Box Plot-Density Trace Synergism,” *Am. Stat.*, vol. 52, no. 2, pp. 181–184, May 1998, doi: 10.1080/00031305.1998.10480559.
- [35] S. Kipp, A. M. Grabowski, and R. Kram, “What determines the metabolic cost of human running across a wide range of velocities?,” *J. Exp. Biol.*, p. jeb.184218, Jan. 2018, doi: 10.1242/jeb.184218.
- [36] C. M. Askling, N. Malliaropoulos, and J. Karlsson, “High-speed running type or stretching-type of hamstring injuries makes a difference to treatment and prognosis,” *Br. J. Sports Med.*, vol. 46, no. 2, pp. 86–87, Feb. 2012, doi: 10.1136/bjsports-2011-090534.

**Assessing lower limb muscle parameters in
high-speed running on different surfaces using
inertial motion capture**

Worksheet

Gustav J. Chatterton

hst-22-idrtek-4-07



Aalborg Universitet
Kandidat i Idrætsteknologi
Kandidatspeciale 2022
Afleveringsdato: 01-06-2022

1 Introduction to the worksheet

The aim of the study was to investigate if muscle-tendon force, power, rate of length change and strain differentiated, when performing a 30-meter sprint test on natural grass (NG), artificial grass (AG) and hard surface (HS).

Inertial motion capture (IMC) combined with musculoskeletal modeling have proven an useful alternative to optical motion capture (OMC) to investigate kinematics, kinetics and muscle parameters [1]–[3]. Hence, it is possible to investigate the parameters related to hamstring injuries for soccer players in their natural environment. Furthermore, it facilitates a greater explanation of the adaptations which occur when performing high-speed running on different surfaces.

This worksheet will provide a more detailed description of the study background, motive and process concerning the study. Additionally, it will incorporate the theoretical and methodological considerations behind the choices made in relation to both the experiment and the data processing.

The study and worksheet are based on a previous semester project by Chatterton et al., where the IMC system was validated in high-speed running. Hence, sections 3 and 4 in the following worksheet, describes similar theoretical considerations as in the previous semester project [4].

2 Study background

2.1 Hamstring injuries in high-speed running:

Hamstring injuries can be separated into two types: a high-speed running type and a stretch type. The stretch type is often seen in less frequent scenarios such as during the process of kicking, whilst the high-speed running type is the most common of all hamstring injuries in soccer [5], [6]. The mechanism of injury related to the high-speed running type is further described based on two theories. The first argues that the injury happens at the initial stance phase, due to the magnitude of the hip extension and knee flexion occurring at the foot strike [7]. The second and most proclaimed theory describes that the injury occurs in the late swing phase. In the late swing phase a deceleration of the knee extension takes place, causing an eccentric contraction of the hamstring muscles, which combined with maximal knee extension and hip flexion results in peak musculotendon force, negative work and peak strain [8]–[11].

2.2 Injury risk of different surfaces:

Non-contact injuries when performing high-speed running are an increasing concern in soccer [12]. In European soccer, reinjury rates ranged from 12-25 % with the time-loss (i.e., days not being able to perform normal sport activity) based on the severity of the injury and the rehabilitation program [6], [10], [13]. The high injury risk and time-loss constitute a large burden for professional soccer clubs in terms of negative impact on club finance and team performance. Studies investigating the effect of running on different surfaces with distinct footwear and its relationship to injuries are inadequate. Subsequently, further research examining these differences would be beneficial for the etiology of hamstring injuries in soccer. However, investigating these differences is merely a small part of the mechanisms related to hamstring injuries.

An important factor associated with hamstring injuries, is the traction on different surfaces and more specifically between surface and shoe. Traction can be divided into translational traction and rotational traction. High rotational traction has been linked with an increased injury rate to the lower extremities. Sideways movement is mentioned as the main factor of these injuries and the majority are located to the foot, ankle and knee, where injuries such as ankle sprains and ACL tears are common [14], [15]. Translational traction has on the other hand not been associated with a higher injury risk, but instead related to sprint performance. One must consider the relationship between obtaining a higher velocity by leaning more forward into the movement and what adaptations are induced. The interaction between two surfaces is often referred to as friction. A friction coefficient between two uniform and rigid surfaces can be found through the Amontons-Coulomb's laws of friction, in which friction is referred to as the resistance to a sliding movement provided by the normal load. However, in more complex scenarios such as shoe-surface interactions, these laws of friction are not adequate [16]. Football boots and the studs attached are made in various ways, which thereby generates an inconsistency in the interaction between surface and shoe. Thereby, the insufficient research examining the injury risk of running on different surfaces and with distinct shoes, accentuates the necessity of adequate methods, such as musculoskeletal modeling, to estimate muscle parameters during high-speed running.

2.3 Kinematic adaptations

The type of running surface is of importance to the lower limb kinematics. When running on surfaces with increased stiffness Hardin et al., found a decreased hip and knee flexion at foot strike [17]. However, Dixon et al, found an increased knee-flexion on the surfaces with the least impact

absorption. Thereby, the current literature observes contradictory kinematic adaptations, which have a great influence on the muscle parameters.

The hamstring muscles are biarticular, meaning an increased hip flexion combined with an increased knee extension would produce the largest strain on the muscles [18]. As explained in section 2.2, running on AG and NG would induce enhancement of forward lean. This would theoretically lead to a higher flexion of the hip. However, to be certain that any kinematic adaptations occur when performing high-speed running on NG, AG and HS, a comparison had to be made. Thereby, a one-way repeated measures (rm) ANOVA illustrated by a SPM plot with corresponding line plots were conducted as in the enclosed manuscript.

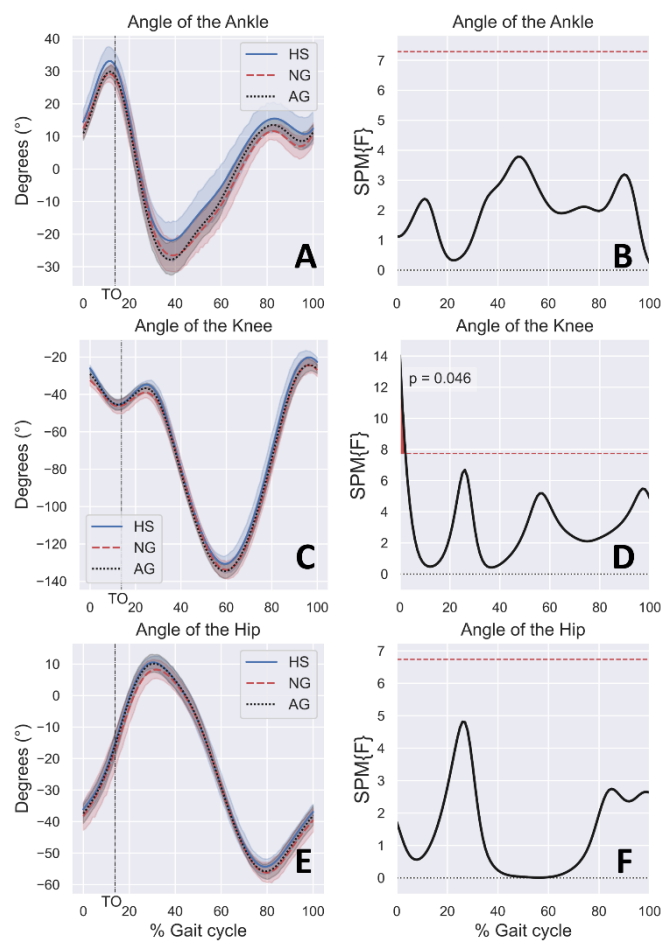


Fig. 1 Mean, SD, and SPM from ankle (A, B), knee (C, D) and hip (E, F) kinematics. The vertical axis for the mean (SD) plots is normalized to degrees and the horizontal axis is normalized to 100 % gait cycle. TO indicates the toe-offset in the gait cycle.

The analysis exhibited no significant differences for the ankle kinematics (Figures 1A and 1B) and for the hip (Figures 1E and 1F). However, the knee kinematics (Figures 1C and 1D) illustrated a

significant difference at the initial foot strike ($p = 0.046$). The post-hoc paired t-test illustrated a significant difference between HS and NG ($p = 0.035$). A more extended knee was present when running on HS compared to NG. Hence, the result of the current study supports the findings by Hardin et al. A more extended knee at foot strike would mean a higher strain on the hamstrings, which is reinforced since no difference is found for the hip flexion. However, no differences were found for the whole swing phase, meaning that no kinematic adaptations occur in the phase predominantly associated with hamstring injuries.

2.4 Methods examining hamstring muscle parameters

When investigating the effects of high-speed running, prior literature have used various methods to assess the hamstring mechanisms related to injuries. One method is electromyography (EMG), which allows the possibility to obtain a direct measurement of muscular activity. Most studies investigating peak muscle activation, found a correlation between increased running speed and peak activation. Furthermore, the time of peak activation during the gait cycle, show different results between studies. Some argue that peak activation is found in the terminal swing phase [19], [20], whereas other studies report the peak activation in the stance phase [21].

In the current project, it was the intention to use EMG on both ST and BFlh. By incorporating a direct measurement of the activation in the hamstring muscles, it would facilitate the possibility of verifying the results of the musculoskeletal modeling. Hence, it would enlighten the debate whether peaks in the muscle parameters occur in the stance phase or in the swing phase. Due to technical issues on the test-day, the EMG system malfunctioned and was excluded from the project.

Using EMG in high-speed running has some limitations. The muscle parameters (i.e., Fout, Pmt, LmtDot and strain) estimated by the musculoskeletal modeling, are not in direct correlation with muscle activity. Despite EMG being a well-used method, complications such as crosstalk can have an effect on the signal [22], [23]. Furthermore, the placement of the EMG electrodes is found by palpation of the specific muscle. Therefore, consistent placement is of great importance and if not placed correctly it could produce inconsistent results.

3 Methodological theory

3.1 Xsens and inertial motion capture

The musculoskeletal model driven by AnyBody Modeling System (AMS), was based on kinematic recordings obtained by the Xsens MVN Link suit, which before implementing to AnyBody was processed in Xsens MVN studio v. 2021.0.1. The Xsens suit incorporates 17 inertial measurement units (IMUs). Each IMU consists of a 3D accelerometer, 3D gyroscope and a 3D magnetometer. The individual IMU is placed in the suit on specific anatomical landmarks on the segment and is connected by a cable system across the body. All signals are collected into the Xbus Master box placed on the back of the participants, which then sends a signal to a Wifi-router connected to a PC. The signals are then live broadcasted in Xsens MVN studio, by visualizing a 3D figure of the participant.

3.2 Calibration, inertial tracking, and joint reduction error

The body dimensions used as input for the musculoskeletal models were manually measured following the Xsens guidelines. Prior to testing, a system calibration was performed, which consisted of standing in a neutral position (N-pose), followed by a short walk, and returning to the N-pose. By performing the N-pose, the rotation of each sensor was obtained by utilizing the actual positioning of the sensors on the specific segments and corresponding it to the orientation in the global reference frame (Figures 2B and 2C). By walking and returning to the N-pose, the positioning and angular velocity was used to define each sensor's initial angle in correspondence to the segment it was attached to. Subsequently, by combining the orientation of two or more sensors with the integrated angular velocity measured with a 3D gyroscope, the angular change can be found (Figure 2D).

To acquire the position of the sensor in the global frame, the accelerometers in the IMUs are utilized. The measurement by the accelerometer contains a vector incorporating the gravitational acceleration and the sensor acceleration. By excluding the gravitational acceleration, the sensor position can be calculated by integrating the acceleration twice [24].

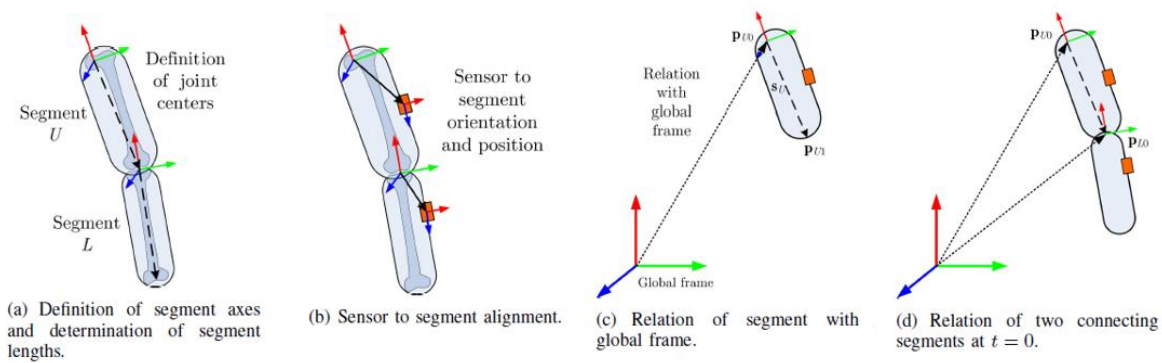


Fig. 2 Definition of segments (U and L) in the global frame [24].

The inertial navigation algorithm (i.e., calculation of position, orientation, and velocity by dead reckoning) can be transformed into segment kinematics, by utilizing a biomechanical model, stating that all segments are connected by joints and that each sensor is attached to a specific segment. An anatomical frame specifies the joint origins which are placed in the functional axes, meaning that the X, Y and Z axis are related to the segment's movement (Figure 2A). Thereby, flexion/extension is determined as the rotation around the Y-axis between to segments, internal/external rotation is around the Z-axis and abduction/adduction around the X-axis.

The 17 IMUs are placed in a manner, that the biomechanical model incorporates 23 segments: toes, feet, lower legs, upper legs, shoulders, upper arms, forearms, hands, pelvis, L5, L3, T8, T12, head and neck. The biomechanical model uses stiffness parameters to estimate the segments, where no IMUs are attached. Furthermore, to reduce uncertainties in the movement of the segment, each joint is determined by specific characteristics, meaning that joints such as the knee are specified as hinged joints, limiting the rotation around the Z and X-axis. The hip joint is specified as a ball and socket joint, allowing movement in all three axes [24].

Following the calculation of the segment kinematics for each frame, an increased uncertainty of the joint position and rotation will emerge (Figure 3A). This uncertainty is developed due to noise and movement of the sensor in respect to its original position. To counteract these unwanted uncertainties, a joint measurement update is implemented utilizing a Kalman filter. In a stepwise process the Kalman filter corrects the kinematic drift and reduces the uncertainties of the joint position (Figure 3B) [24]. Subsequently, the section above illustrates how the calibration of the IMC system advances from inertial tracking of each sensor, to calculating the kinematics between segments and finally to remove unwanted errors.

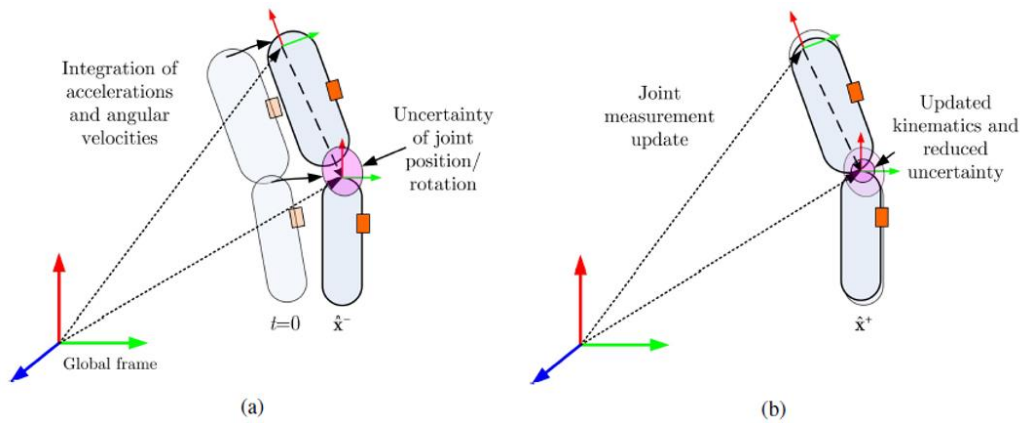


Fig 3. The joint measurement update with implementation of the Kalman filter [24].

4 Musculoskeletal modeling

4.1 Implementation to AnyBody Modelling System

The musculoskeletal model made in AMS, is an inverse dynamics approach, which is constructed by recorded kinematics and boundary conditions set to balance the model, which incorporate internal and external forces. The process from recording kinematic data with IMC, to estimating muscle parameters in AMS, follows a chronological order (Figure 4), which in the following sections will be described.

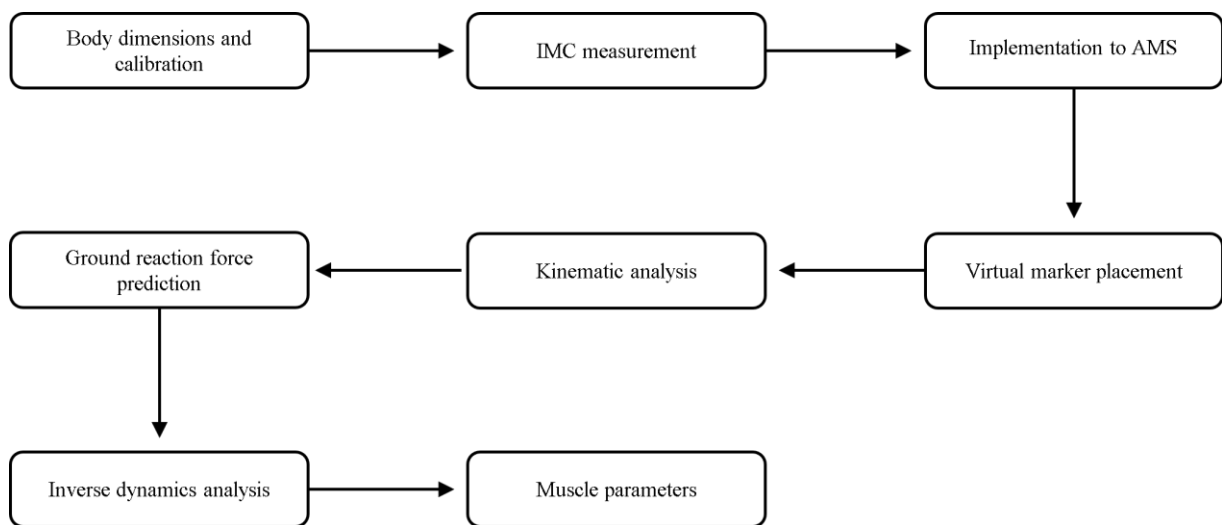


Fig 4. Chronological order from IMC recordings to estimating muscle parameters.

The data recorded by the IMC system, was exported as a Biovision Hierarchy file (.BVH) and contained the stick figure, embracing the 23 defined segments with corresponding kinematics. For the stick figure to correspond with the musculoskeletal model driven in AMS, 28 virtual markers were introduced to specific anatomical placements. Hereafter, the virtual markers were considered as experimental markers, allowing the possibility of marker tracking [1].

4.2 Kinematic and inverse dynamics analysis

Prior to the inverse dynamics analysis, the experimental markers are tracked in all frames and subsequently saved as joint angles with respect to time. The saved joint angles from the marker tracking are combined with the external forces from the GRF prediction and used to drive the inverse dynamics analysis. To estimate internal moments and joint reaction forces, an equilibrium equation states;

$$Cf = d$$

The equation incorporates C, which embraces the constants of the model structure and f represents all unknown internal forces. For the model to obtain equilibrium, d contains all external forces [1], [25].

4.3 Muscle recruitment

When using an inverse dynamics approach to estimate muscle forces, a muscle recruitment problem will occur, due to the body having more muscles than degrees-of-freedom. The external forces affecting the body, will produce internal forces, which are distributed across multiple muscles. However, when multiple muscles are involved, an uncertainty occurs when estimating the internal force. This uncertainty arises because the equilibrium equation has more unknown parameters than equations, meaning boundless solutions. However, muscle recruitment has through known movements proven to be systematically chosen, based on the muscle activations made by the central nervous system [26]. To obtain equilibrium an optimization function is formulated, which by constraints can choose the correct solution.

$$\begin{aligned} & \text{minimize } G(f^M) \\ & \text{subject to } cf = d \\ & f_i^M \geq 0, i = 1 \dots, n^M \end{aligned}$$

In the formulation above, the cost function G , is minimized by the set of muscle forces f^M . To obtain equilibrium the function is constrained, so muscle forces F_i^M only can be positive and that muscle forces have metabolism, meaning an energy consumption should be minimized. Additionally, the function is established on the important aspect, that muscles only are capable of pulling and not pushing [1], [25], [27].

In the current study the cost function G , was further specified as a quadratic polynomial function, meaning a higher synergism between muscles

$$G(f^M) = \sum_{i=1}^{n^M} \left(\frac{f_i^M}{N_i} \right)^2$$

The polynomial function is expressed by F_i^M which is the i 'th muscle force, N_i indicates the strength of the i 'th muscle and n^M expresses the number of muscles. The order of the function determines the synergism between the muscles. A low order generates unrealistic results since stronger muscles perform the majority of the work. The maximum order in AMS is 5, since too high orders also can cause numeric instability. When using the BVH_Xsens templates in AMS, the default order is 2. A higher order would possibly generate a higher synergism between muscles, meaning a different result and possibly lower F_{out} for BFlh and ST. However, the AMS template will not operate with higher orders for the BVH_Xsens model [2], [25].

4.4 Ground reaction force prediction

For the musculoskeletal model to predict muscle parameters during the stance phase, a ground reaction force (GRF) prediction was introduced. The GRF prediction has been proven a useful alternative to traditional force plates [1], [2], [27], [28]. The current study used a modified version of the GRF prediction introduced by Skals et al. [27] Hence, 25 contact nodes were placed under each foot in the model, generating normal and frictional forces. To ensure activation of the contact nodes, a detection volume with an upper (LimitDistHigh) and lower (LimitDistLow) bound was set. Furthermore, a velocity threshold (LimitVelHigh) was introduced, meaning that the contact nodes would be activated if inside the threshold. Chatterton et al., validated the IMC system and GRF prediction during high-speed running. By comparing the settings of the GRF prediction with actual

force plates, the correct adjustments of each threshold were extrapolated. By setting the bound of LimitDistHigh and LimitDistLow to 0.04 meters and LimitVelHigh to 2 m/s, the most accurate prediction was found [29].

However, one parameter that was not adjusted in the study by Chatterton et al., was the FrictionCoefficient. The 25 contact nodes each embraced five uniaxial force actuators. One of the force actuators was aligned with the vertical axis, two with anteroposterior axis and two with the mediolateral axis. The actuator positioned with the vertical axis generated a normal force, while the actuators for the remaining axes could generate positive and negative friction forces. The four actuators could generate a force in the normal direction and simultaneously generate a force in one of the positive or negative anteroposterior - and mediolateral directions. Thereby, when a force was generated in the normal direction, the four actuators were organized so they also would generate a shear force adjusted by the FrictionCoefficient. Hence, the normal force for each contact node during the stance phase is estimated by the sum of five normal forces and concurrently the magnitude of the frictional force is constricted by the normal force [27].

In the current study, the participants performed high-speed running on three different surfaces. As mentioned in section 2.2, estimating the friction coefficient between surfaces and shoe can be difficult. Hence, it was argued that traction would be a better representation in complex scenarios such as the interaction between NG and football boots with studs. In a study by Shorten & Himmelsbach, a translational traction coefficient was estimated for different surfaces with different shoes, by utilizing force plates. The study illustrated a traction coefficient of 0.5 for HS, 0.95 for NG and 1.3 for AG, which were implemented in the current study. These values were obtained by visually inspecting a graph, since they were not presented in the results [16]. The default settings in AMS for the FrictionCoefficient is 0.5 and to determine if changing the settings for NG and AG would affect the GRF prediction, a comparison was made. Subsequently, the GRF predictions in the vertical, mediolateral, and anteroposterior directions were visualized with line plots (Figures 5A,5C,6A,6C,7A and 7C) and the differences analyzed by a one-way (rm) ANOVA (Figures 5B,5D,6B,6D,7B and 7D).

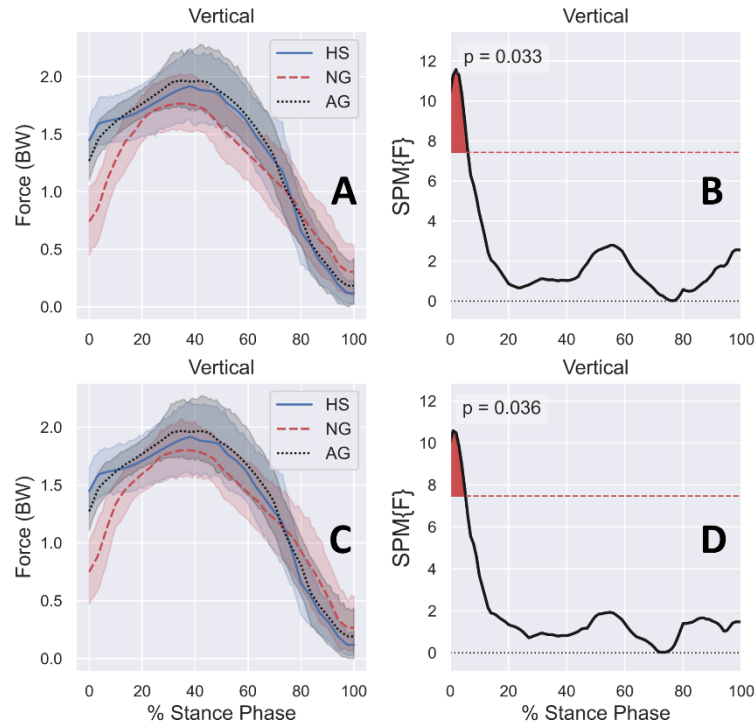


Fig. 5 Mean, SD, and SPM from the vertical GRF predictions with alternated FrictionCoefficient (A & B) and default settings (C & D). The vertical axis for the mean (SD) plots are normalized to force (BW) and the horizontal axis is normalized to 100 % stance phase.

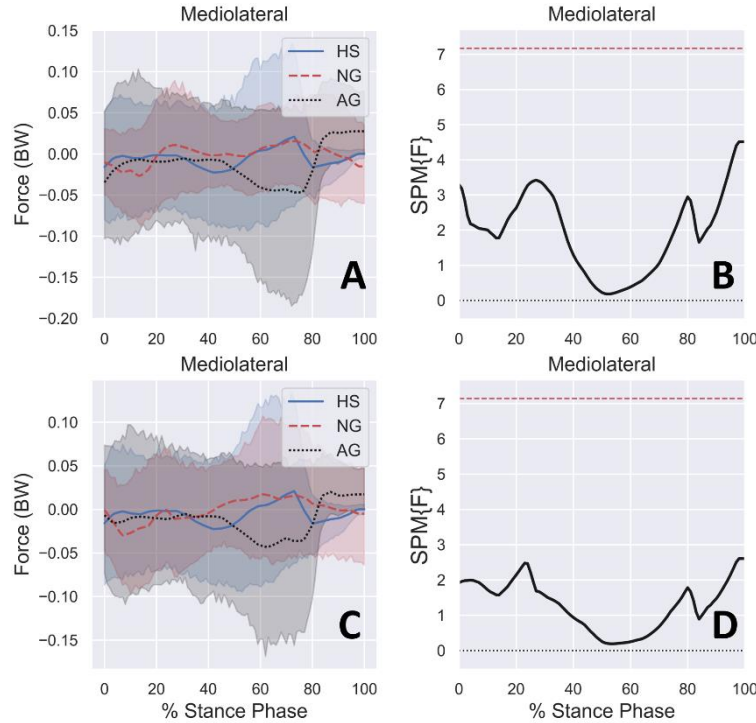


Fig. 6 Mean, SD and SPM from the mediolateral GRF prediction with alternated FrictionCoefficient (A & B) and default settings (C & D). The vertical axis for the mean (SD) plots are normalized to force (BW) and the horizontal axis is normalized to 100 % stance phase.

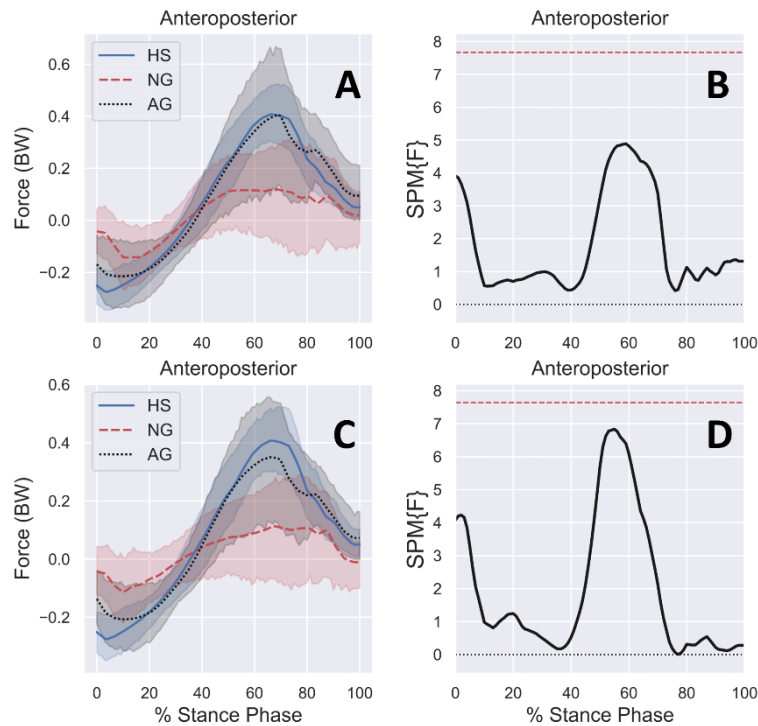


Fig. 7 Mean, SD and SPM from the Anteroposterior GRF prediction with alternated FrictionCoefficient (A & B) and default settings (C & D). The vertical axis for the mean (SD) plots are normalized to force (BW) and the horizontal axis is normalized to 100 % stance phase.

Figures A and B represent the alternated FrictionCoefficient, whilst Figures C and D illustrate the default settings. By visually inspecting the figures, no major differences can be seen. The vertical GRF prediction exhibits a slightly higher difference in the p-value at foot strike. The Mediolateral prediction illustrates slightly higher SDs and the anteroposterior shows a slight alteration of the predicted GRF for NG, meaning a smaller difference in peak GRF around 60 % of the gait cycle. Thereby, the alteration of the FrictionCoefficient did not develop any major changes in the GRF prediction. This illustrates that modifications of the model need further studies. In the current model, the foot characteristics are somewhat insufficient. The foot is currently modeled without shoes, meaning that the stiffness of the specific footwear is not incorporated. Furthermore, the foot is modeled as a stiff segment, meaning two contacts to the ground occur in one stance phase. In a real scenario the foot would embrace a more rolling movement on the ground. Thereby, this indicates that further study regarding the foot model is needed, to improve the GRF prediction.

5 Methodological considerations

5.1 Study population

In the current study the participants consisted of male/youth soccer players from FC-Midtjylland's talent academy and a smaller club Ikast FC. The average age in the study was 18.2 years \pm 1.15, meaning that all players either played in the U17 or U19 league. When investigating the etiology of hamstring injuries, prior studies have emphasized that multiple physical parameters are related to an increased risk of sustaining injuries. Increased age has been associated with the risk of sustaining hamstring injuries, due to lower quadriceps flexibility, decreased hip flexion range of motion and reduced eccentric hamstring strength [30]–[32]. Age above 23 years have been linked with higher risks and the odds of sustaining a hamstring injury have proven to increase each year after reaching the age of 23. Additionally, previous injury history have been linked with both age and higher injury risk [30], [31]. In the current study, an exclusion criterion was established, stating that no history of injuries the last six months was accepted.

A more diverse study population in the current study, could have affected the results. Maximum running speed and acceleration is age related, meaning that a more mature population could have resulted in an increased running speed [33]. Hence, when the magnitude of L_{mtDot} and P_{mt} is dependent on running speed, an increase could have induced different results.

5.2 Dominant versus non dominant leg

When assessing injury risk in soccer, one must consider the influence of the dominant versus non dominant leg. The dominant leg is determined as the kicking leg and is therefore used more frequently in soccer due to the high amount of passing and shooting the ball. The dominant leg has been related to higher risk of sustaining hamstring injuries across age groups and gender. Hence, it has been argued that when investigating scenarios related to hamstring injuries, an adjustment of leg dominance should be conducted [34], [35]. Subsequently, in the current study it was chosen to analyze the dominant leg of each participant, meaning an adjustment in the data-processing. Seven of the twelve participants were right leg dominant, which resulted in an adjustment of the mediolateral GRF for the five left leg dominant participants.

5.3 Footwear

When performing high-speed running on different surfaces, both the performance and injury risk are dependent on the traction. The traction is dependent on both the surfaces and the shoe. Specific shoes

have been made for the different surfaces (i.e., running shoes for HS, football boots for NG and turf boots for AG). To obtain higher performance a higher translational and rotational traction is wanted. Thomson et al., investigated multiple football boots and turf boots on NG and AG and illustrated significant differences in rotational traction between the boots. Football boots exhibited a higher rotational traction on both NG and AG [14]. However, a higher rotational traction has been related with higher injury risks [15]. Thereby, a cost-benefit analysis between performance and injury risk must be made, when determining which boots should be used. In the current study, it would have enhanced the ecological validity to use football boots on NG and turf boots on AG. However, not all participants owned turf boots, meaning football boots were used for both NG and AG. The participants all used different football boots, meaning that a confounder was present. By using different boots, the traction was not the same for all participants. Additionally, each of the boots possess different stiffness properties, which thereby also decreases the reliability of the results.

5.4 Surface conditions

Important parameters for surface traction are the hardness, dryness and grass coverage of the field played upon. The condition of the surface is dependent on weather conditions, and weather conditions prior to the test days. Furthermore, a reduced traction caused by turf softening and water on the field, reduced the risk of lower limb injuries [36]. The investigation took place from March to April in Ikast, Denmark. Since rain could affect both the surface properties and the possibility of using test-equipment outdoors, no trials were conducted if it had been raining either the day before or on the test day. One of the participant's trials were thus excluded due to the weather conditions.

5.5 The 30-meter sprint test

In the current study, it was chosen that participants should perform an all-out 30-meter sprint test. Most sprints performed in soccer games are between 9.9 and 32.5 meters and the standard length of sprint tests performed in soccer clubs are 30 meters [37]. However, one factor which had to be considered was the running speed. Studies investigating either kinematics, musculoskeletal parameters or physiological effects often perform the test under controlled running speeds or controlled settings (i.e., treadmills and laboratory settings) [1], [27], [29], [38]. However, hamstring injuries in soccer occur on the fields where matches and practices are conducted. Furthermore, the injuries happen under non-controlled speeds and have been related to increased running speed [39]. Subsequently, to enhance the ecological validity of the study, it was chosen that the participants

should perform all out sprint tests, without controlling their speed. This meant that the parameters Fout, Pmt, LmtDot and strain all would be affected by running speed, meaning that a direct correlation to an increase in the parameters could not be shown with regards to the surface. However, if one surface allows the possibility to obtain higher running speeds as for AG, it is feasible that an increase of the muscle parameters is related to the surface.

5.6 Low-pass filter

When using kinematic data from high-speed running as input for musculoskeletal modeling, the appropriate filter type, order, and cut-off frequency must be chosen. Examining high-speed running presents a greater challenge for data acquisitions compared to other movements, due to the higher velocities and impacts during running. Chatterton et al., conducted a validation of IMC and GRF prediction compared to OMC and force plates [29]. By examining previous studies investigating kinematics in sprinting, a cut-off frequency between 10 and 20 Hz was found appropriate [40], [41]. Subsequently, an evaluation of cut-off frequencies between 10 and 20 Hz and their impact on the results was conducted. Hence, a low-pass 2nd order Butterworth filter, with a cut-off frequency of 15 Hz was chosen in both the current study and the validation study [29].

5.7 Statistical considerations

Muscle-tendon force, power, rate of length change and strain are continuous data and were presented with mean (SD) in a Seaborn line plot. A one-way (rm) ANOVA was used to analyze if any difference in the muscle parameters occurred between the three surfaces. The statistical analysis was conducted using a one-dimensional, one-tailed statistical parametric mapping (SPM) with the alpha level set to 5%. When analyzing continuous data, SPM produces a greater visual representation of the ANOVA, by illustrating the magnitude of the differences in plots [42]. The one-way (rm) ANOVA exclusively show that a significant difference is found, but not in-between which groups. Therefore, a post-hoc paired t-test had to be conducted with an alpha level of 5%. The one-way (rm) ANOVA default settings was one-tailed and could not be changed, whilst the paired t-test was two-tailed. A two-tailed t-test investigates for any differences in both directions of the mean value. Thereby, a two-tailed t-test examines if the mean of one group both is above or below the other group. However, when analyzing for differences in both directions the probability distribution of 5% is divided into 2.5% for each direction. The one-tailed ANOVA investigates in one direction, meaning that all 5% of the

probability distribution is used to examine one direction. In the article of the current study a significant difference was found by the one-tailed ANOVA for BFlh Pmt, but no difference was found in the two-tailed t-test. If inspecting the figure (Figure 4B in the article), the difference found is relatively small. Thereby, when removing 2.5 % of the probability distribution, this would explain why no difference is found for the two-tailed t-test [43].

References

- [1] A. Karatsidis *et al.*, “Predicting kinetics using musculoskeletal modeling and inertial motion capture,” *ArXiv180101668 Phys.*, Jan. 2018, Accessed: Oct. 27, 2021. [Online]. Available: <http://arxiv.org/abs/1801.01668>
- [2] F. G. Larsen, F. P. Svenningsen, M. S. Andersen, M. de Zee, and S. Skals, “Estimation of Spinal Loading During Manual Materials Handling Using Inertial Motion Capture,” *Ann. Biomed. Eng.*, vol. 48, no. 2, pp. 805–821, Feb. 2020, doi: 10.1007/s10439-019-02409-8.
- [3] J.-T. Zhang, A. C. Novak, B. Brouwer, and Q. Li, “Concurrent validation of Xsens MVN measurement of lower limb joint angular kinematics,” *Physiol. Meas.*, vol. 34, no. 8, pp. N63–N69, Aug. 2013, doi: 10.1088/0967-3334/34/8/N63.
- [4] G. Chatterton, N. Kristiansen, N. Kunwald, and H. Jesper, “Estimating Biceps Femoris long head mechanisms in high speed running using inertial motion capture,” *Unpublished*, vol. 2022.
- [5] C. M. Askling, N. Malliaropoulos, and J. Karlsson, “High-speed running type or stretching-type of hamstring injuries makes a difference to treatment and prognosis,” *Br. J. Sports Med.*, vol. 46, no. 2, pp. 86–87, Feb. 2012, doi: 10.1136/bjsports-2011-090534.
- [6] J. Ekstrand, M. Hägglund, and M. Waldén, “Epidemiology of Muscle Injuries in Professional Football (Soccer),” *Am. J. Sports Med.*, vol. 39, no. 6, pp. 1226–1232, Jun. 2011, doi: 10.1177/0363546510395879.
- [7] R. Mann and P. Sprague, “A Kinetic Analysis of the Ground Leg During Sprint Running,” *Res. Q. Exerc. Sport*, vol. 51, no. 2, pp. 334–348, May 1980, doi: 10.1080/02701367.1980.10605202.
- [8] A. Danielsson *et al.*, “The mechanism of hamstring injuries – a systematic review,” *BMC Musculoskelet. Disord.*, vol. 21, no. 1, p. 641, Dec. 2020, doi: 10.1186/s12891-020-03658-8.
- [9] C. J. B. Kenneally-Dabrowski, N. A. T. Brown, A. K. M. Lai, D. Perriman, W. Spratford, and B. G. Serpell, “Late swing or early stance? A narrative review of hamstring injury mechanisms during high-speed running,” *Scand. J. Med. Sci. Sports*, vol. 29, no. 8, pp. 1083–1091, Aug. 2019, doi: 10.1111/sms.13437.
- [10] J. Petersen, K. Thorborg, M. B. Nielsen, E. Budtz-Jørgensen, and P. Hölmich, “Preventive Effect of Eccentric Training on Acute Hamstring Injuries in Men’s Soccer: A Cluster-Randomized Controlled Trial,” *Am. J. Sports Med.*, vol. 39, no. 11, pp. 2296–2303, Nov. 2011, doi: 10.1177/0363546511419277.
- [11] B. Yu, R. M. Queen, A. N. Abbey, Y. Liu, C. T. Moorman, and W. E. Garrett, “Hamstring muscle kinematics and activation during overground sprinting,” *J. Biomech.*, vol. 41, no. 15, pp. 3121–3126, Nov. 2008, doi: 10.1016/j.jbiomech.2008.09.005.
- [12] H. Nobari, E. Mainer-Pardos, A. Denche Zamorano, T. G. Bowman, F. M. Clemente, and J. Pérez-Gómez, “Sprint Variables Are Associated with the Odds Ratios of Non-Contact Injuries

- in Professional Soccer Players,” *Int. J. Environ. Res. Public Health*, vol. 18, no. 19, p. 10417, Oct. 2021, doi: 10.3390/ijerph181910417.
- [13] C. M. Askling and B. C. Heiderscheit, “Acute Hamstring Muscle Injury: Types, Rehabilitation, and Return to Sports,” in *Sports Injuries*, M. N. Doral and J. Karlsson, Eds. Berlin, Heidelberg: Springer Berlin Heidelberg, 2015, pp. 2137–2147. doi: 10.1007/978-3-642-36569-0_171.
- [14] A. Thomson, C. Bleakley, W. Holmes, E. Hodge, D. Paul, and J. W. Wannop, “Rotational traction of soccer football shoes on a hybrid reinforced turf system and natural grass,” *Footwear Sci.*, vol. 14, no. 1, pp. 58–69, Jan. 2022, doi: 10.1080/19424280.2022.2038690.
- [15] J. Wannop, “Footwear traction and lower extremity non-contact injury,” 2012, doi: 10.11575/PRISM/26204.
- [16] M. R. Shorten and J. A. Himmelsbach, “Shorten, M.R., Hudson, B., & Himmelsbach, J.A. (2002). SHOE-SURFACE TRACTION OF CONVENTIONAL AND IN-FILLED SYNTHETIC TURF FOOTBALL SURFACES,” 2002.
- [17] E. C. Hardin, A. J. Van Den Bogert, and J. Hamill, “Kinematic Adaptations during Running: Effects of Footwear, Surface, and Duration:,” *Med. Sci. Sports Exerc.*, pp. 838–844, May 2004, doi: 10.1249/01.MSS.0000126605.65966.40.
- [18] D. G. Thelen, E. S. Chumanov, T. M. Best, S. C. Swanson, and B. C. Heiderscheit, “Simulation of biceps femoris musculotendon mechanics during the swing phase of sprinting,” *Med. Sci. Sports Exerc.*, vol. 37, no. 11, pp. 1931–1938, Nov. 2005, doi: 10.1249/01.mss.0000176674.42929.de.
- [19] A. Higashihara, T. Ono, J. Kubota, T. Okuwaki, and T. Fukubayashi, “Functional differences in the activity of the hamstring muscles with increasing running speed,” *J. Sports Sci.*, vol. 28, no. 10, pp. 1085–1092, Aug. 2010, doi: 10.1080/02640414.2010.494308.
- [20] H. Kyrolainen, P. V. Komi, and A. Belli, “Changes in Muscle Activity Patterns and Kinetics With Increasing Running Speed,” *J. Strength Cond. Res.*, vol. 13, no. 4, p. 400, 1999, doi: 10.1519/1533-4287(1999)013<0400:CIMAPA>2.0.CO;2.
- [21] S. Jönhagen, M. O. Ericson, G. Németh, and E. Eriksson, “Amplitude and timing of electromyographic activity during sprinting,” *Scand. J. Med. Sci. Sports*, vol. 6, no. 1, pp. 15–21, Jan. 2007, doi: 10.1111/j.1600-0838.1996.tb00064.x.
- [22] T. W. Kaminski and T. D. Royer, “Electromyography and Muscle Force: Caution Ahead,” *Athl. Ther. Today*, vol. 10, no. 4, pp. 43–45, Jul. 2005, doi: 10.1123/att.10.4.43.
- [23] A. G. Schache, T. W. Dorn, P. D. Blanch, N. A. T. Brown, and M. G. Pandy, “Mechanics of the Human Hamstring Muscles during Sprinting,” *Med. Sci. Sports Exerc.*, vol. 44, no. 4, pp. 647–658, Apr. 2012, doi: 10.1249/MSS.0b013e318236a3d2.
- [24] D. Roetenberg, H. Luinge, and P. Slycke, “Xsens MVN : Full 6DOF Human Motion Tracking Using Miniature Inertial Sensors,” *Xsens Motion Technol. BV Tech Rep*, no. 1, 2009.
- [25] M. Damsgaard, J. Rasmussen, S. T. Christensen, E. Surma, and M. de Zee, “Analysis of musculoskeletal systems in the AnyBody Modeling System,” *Simul. Model. Pract. Theory*, vol. 14, no. 8, pp. 1100–1111, Nov. 2006, doi: 10.1016/j.simpat.2006.09.001.
- [26] A. Erdemir, S. McLean, W. Herzog, and A. J. van den Bogert, “Model-based estimation of muscle forces exerted during movements,” *Clin. Biomech.*, vol. 22, no. 2, pp. 131–154, Feb. 2007, doi: 10.1016/j.clinbiomech.2006.09.005.
- [27] S. Skals, M. K. Jung, M. Damsgaard, and M. S. Andersen, “Prediction of ground reaction forces and moments during sports-related movements,” *Multibody Syst. Dyn.*, vol. 39, no. 3, pp. 175–195, Mar. 2017, doi: 10.1007/s11044-016-9537-4.
- [28] R. Fluit, M. S. Andersen, S. Kolk, N. Verdonschot, and H. F. J. M. Koopman, “Prediction of ground reaction forces and moments during various activities of daily living,” *J. Biomech.*, vol. 47, no. 10, pp. 2321–2329, Jul. 2014, doi: 10.1016/j.jbiomech.2014.04.030.

- [29] G. J. Chatterton, J. B. Hansen, N. H. Kristiansen, N. P. Kunwald, U. G. Kersting, and A. S. Oliveira, "ASSESSING KINEMATICS AND KINETICS OF HIGH-SPEED RUNNING USING INERTIAL MOTION CAPTURE: A PRELIMINARY ANALYSIS," *ISBS Proceedings Archive*, vol. 2022, Appendix A.
- [30] B. J. Gabbe, "Risk factors for hamstring injuries in community level Australian football," *Br. J. Sports Med.*, vol. 39, no. 2, pp. 106–110, Feb. 2005, doi: 10.1136/bjsm.2003.011197.
- [31] G. Henderson, C. A. Barnes, and M. D. Portas, "Factors associated with increased propensity for hamstring injury in English Premier League soccer players," *J. Sci. Med. Sport*, vol. 13, no. 4, pp. 397–402, Jul. 2010, doi: 10.1016/j.jsams.2009.08.003.
- [32] J. Vicens-Bordas *et al.*, "ECCENTRIC HAMSTRING STRENGTH IS ASSOCIATED WITH AGE AND DURATION OF PREVIOUS SEASON HAMSTRING INJURY IN MALE SOCCER PLAYERS," *Int. J. Sports Phys. Ther.*, vol. 15, no. 2, pp. 246–253, Apr. 2020, doi: 10.26603/ijsp20200246.
- [33] A. Mendez-Villanueva, M. Buchheit, S. Kuitunen, A. Douglas, E. Peltola, and P. Bourdon, "Age-related differences in acceleration, maximum running speed, and repeated-sprint performance in young soccer players," *J. Sports Sci.*, vol. 29, no. 5, pp. 477–484, Mar. 2011, doi: 10.1080/02640414.2010.536248.
- [34] M. D. DeLang *et al.*, "The dominant leg is more likely to get injured in soccer players: systematic review and meta-analysis.," *Biol. Sport*, vol. 38, no. 3, pp. 397–435, 2021, doi: 10.5114/biolSport.2021.100265.
- [35] K. Svensson, M. Eckerman, M. Alricsson, T. Magounakis, and S. Werner, "Muscle injuries of the dominant or non-dominant leg in male football players at elite level," *Knee Surg. Sports Traumatol. Arthrosc.*, vol. 26, no. 3, pp. 933–937, Mar. 2018, doi: 10.1007/s00167-016-4200-4.
- [36] J. Orchard, "Is There a Relationship Between Ground and Climatic Conditions and Injuries in Football?," *Sports Med.*, vol. 32, no. 7, pp. 419–432, 2002, doi: 10.2165/00007256-200232070-00002.
- [37] A. Ferro, J. Villacieros, P. Floría, and J. L. Graupera, "Analysis of Speed Performance In Soccer by a Playing Position and a Sports Level Using a Laser System," *J. Hum. Kinet.*, vol. 44, no. 1, pp. 143–153, Dec. 2014, doi: 10.2478/hukin-2014-0120.
- [38] A. Sassi, A. Stefanescu, P. Menaspa', A. Bosio, M. Riggio, and E. Rampinini, "The Cost of Running on Natural Grass and Artificial Turf Surfaces," *J. Strength Cond. Res.*, vol. 25, no. 3, pp. 606–611, Mar. 2011, doi: 10.1519/JSC.0b013e3181c7baf9.
- [39] E. S. Chumanov, B. C. Heiderscheit, and D. G. Thelen, "Hamstring Musculotendon Dynamics during Stance and Swing Phases of High-Speed Running," *Med. Sci. Sports Exerc.*, vol. 43, no. 3, pp. 525–532, Mar. 2011, doi: 10.1249/MSS.0b013e3181f23fe8.
- [40] R. Jacobs and G. J. van Ingen Schenau, "Intermuscular coordination in a sprint push-off," *J. Biomech.*, vol. 25, no. 9, pp. 953–965, Sep. 1992, doi: 10.1016/0021-9290(92)90031-U.
- [41] J. P. Hunter, R. N. Marshall, and P. J. McNair, "Segment-interaction analysis of the stance limb in sprint running," *J. Biomech.*, vol. 37, no. 9, pp. 1439–1446, Sep. 2004, doi: 10.1016/j.jbiomech.2003.12.018.
- [42] T. C. Pataky, "Generalized n-dimensional biomechanical field analysis using statistical parametric mapping," *J. Biomech.*, vol. 43, no. 10, pp. 1976–1982, Jul. 2010, doi: 10.1016/j.jbiomech.2010.03.008.
- [43] J. H. Zar, *Biostatistical analysis*. 2014. Accessed: May 27, 2022. [Online]. Available: <http://search.ebscohost.com/login.aspx?direct=true&scope=site&db=nlebk&db=nlabk&AN=1418297>